Structure and Orientation Changes of ω-and γ-Gliadins at the Air-Water Interface: A PM-IRRAS Spectroscopy and Brewster Angle Microscopy Study

Amélie Banc, B. Desbat, Denis Renard, Yves Popineau, Cécile Mangavel, Laurence Navailles

Structure and Orientation Changes of ω- and γ-Gliadins at the Air-Water Interface: A PM-IRRAS Spectroscopy and Brewster Angle Microscopy Study

Amélie Banc[†], Bernard Desbat[‡], Denis Renard[§], Yves Popineau[§], Cécile Mangavel[§], and Laurence Navailles*[†]

†*Centre de Recherche Paul Pascal, UPR 8641-CNRS, Avenue Albert Schweitzer, F-33600 Pessac,*
‡*Laboratoire de Chimie et Biologie des Membranes et Nanoobjets, UMR 5248-CNRS, Universite´ Bordeaux 1, ENITAB, 2 rue Robert Escarpit, F-33607 Pessac,*
§*UR1268 Biopolymères Interactions Assemblages, INRA, F-44300 Nantes.*

Microscopic and molecular structures of ω- and γ-gliadin monolayers at the air-water interface were studied under compression by three complementary techniques: compression isotherms, polarization modulation infrared reflection absorption spectroscopy (PM-IRRAS), and Brewster angle microscopy (BAM). For high molecular areas, gliadin films are homogeneous, and a flat orientation of secondary structures relative to the interface is observed. With increasing compression, the nature and orientation of secondary structures changed to minimize the interfacial area. The γ-gliadin film is the most stable at the air-water interface; its interfacial volume is constant with increasing compression, contrary to ω-gliadin films whose molecules are forced out of the interface. γ-gliadin stability at a high level of compression is interpreted by a stacking model.

Introduction

Wheat storage proteins (WSP), constituting gluten, are very important for various technological applications ranging from baking performance[1] to the elaboration of biomaterials[2] and the development of new drug delivery systems[3].

Naturally, these proteins serve as an amino acid source for germination. In developing grains, these proteins are located in the endosperm cells, transiently stored as protein bodies[4]. These bodies are micrometer-sized organelles emerging from endoplasmic reticulum membranes and may contain up to 80% protein. The mechanisms leading to the formation of the protein bodies and the organization of storage proteins inside the organelles are not well understood today[5], whereas they are key parameters of wheat grain quality.

Most WSPs are classified as prolamins because of their high proportions of proline and glutamine. Despite their high proportion of polar glutamine residues, prolamins are poorly soluble in water. However, they can be solubilized in water-alcohol mixtures or in low pH solutions. WSPs display very extensive polymorphism, but repeated amino acid sequences are present in all of them. Prolamins are subdivided into two groups on the basis of their ability to form polymeric systems by means of intermolecular disulfide bonds between protein subunits[6]. Gliadins are monomeric proteins, whereas glutenins are polymeric ones. Gliadins account for about half of the gluten proteins and are subdivided into four types according to their electrophoretic mobility in acid-polyacrylamide gel electrophoresis, commonly denoted as α, β, γ-, and ω-gliadins. α, β, and γ-gliadins have similar primary structures. They are composed of a short N-terminal domain, a repetitive domain that contains repeated motifs rich in proline, glutamine, and phenylalanine, and a non-repetitive domain that includes all intramolecular disulfide bonds. The non-repetitive domain is more hydrophobic than the repetitive one, suggesting an amphiphilic feature of these gliadins. ω-gliadins principally consist of proline and glutamine residues and are made up almost entirely of repeated sequences without cysteines to form disulfide bonds[7]. ω-gliadins are globally more polar than α, β, and γ-gliadins[8]. Note that all gliadins contain very few ionic amino acids.

Albeit gluten proteins were studied for a long time, the secondary and tertiary structures of these cereal grain proteins are not well defined. They have not yet been crystallized for X-ray diffraction analysis, and their NMR structure determinations present numerous problems because of their high molecular weight, their extensive repeats, and the large number of prolines in their primary structure[9]. Numerous spectroscopic studies have provided information concerning the secondary structure of whole gluten[10-12] or of some specific constituents[13-17] but always in the bulk and mainly in non-physiological solvents. In all of these studies, the secondary structures of gliadins were found to be very sensitive to environmental conditions such as solvent, hydration, and temperature.

The self-assembly of proteins occurs in a large number of cellular mechanisms and processing conditions related to food and non-food products. Interfacial properties of WSP are essential to understand their biological self-assembly as well as the baking performance of gluten and wheat flour doughs.[18] Prolamins are synthesized, folded, and further accumulated in the aqueous environment of the endoplasmic reticulum of the endosperm cells where membrane surfaces are highly developed. In the wheat dough, prolamins are principally located in the bulk of the gluten network but also at the interface of the air bubbles incorporated by mixing and the carbon dioxide bubbles generated by yeast fermentation. They are thus susceptible to participate to the stabilization of the alveolar structure of baked products[18].

Several studies have been performed at the air-water[19,20] and air-solid interfaces.[21-23] The ability of gliadins to significantly reduce the surface tension of the air-water interface has been reported,[19] but to our knowledge, their structure at these interfaces has never been studied.

The physicochemical mechanisms involved in the formation of the protein bodies in wheat endosperm cells are not yet understood. For this purpose, we used a 2D approach to investigate the self-assembly of prolamins at interfaces in an

aqueous environment. As recently stated in the case of amyloid-like peptides, the 2D approach is a relevant method for studying the aggregation of proteins and peptides,[24] speeding up their aggregation.[25] This approach also permits us to mimic the aggregation process that occurs in vivo in aqueous solutions. Compression of the monolayer is employed to bring the molecules into close contact, as required for the self-assembly processes, and the structure of the proteins can be characterized at different stages. Monolayer compression in the 2D experimental approach thus represents an elegant way to mimic macromolecular crowding occurring in different cell compartments.

In the present work, Langmuir isotherms coupled with Brewster angle microscopy (BAM) and polarization modulation infrared reflection absorption (PM-IRRAS) were collected to investigate in situ γ- and ω-gliadin microscopic and molecular structures. In this study, γ-gliadin serves as a model of cysteine-rich monomeric prolamins, and ω-gliadin serves as a model of cysteine-poor, fully repetitive prolamins. The latter may also help us to understand the contribution of the repetitive sequence of γ-gliadin to the self-assembly mechanism.

Table 1. Main Characteristics of the γ- and ω-Gliadins

	MM (Da) from mass spectrometry	AA composition (residues/molecule[a–c])
γ-gliadin	35 185 (308 residues/molecule)	Gln: 111 Pro: 54 Phe: 15 Lys: 2 Cys: 8 (4 disulfide bridges)
ω-gliadin	42 734 (366 residues/molecule)	Gln: 164 Pro: 106 Phe: 28 Lys: 2 Cys: 0

[a] Muller, S.; Wieser, H.; Popineau, Y. *J. Cereal Sci.* **1998**, 27, 23-25. [b] Popineau, Y.; Pineau, F. *J. Cereal Sci*. **1985,** 3, 363-378. [c] Popineau, Y.; Le Guerroue´ J. L.; Pineau, F. *Lebensm. Wiss. Uni*V. *Technol*. **1986** 19, 266-271.

Experimental Section

Materials. γ– and ω–gliadins were purified from Hardi wheat cultivar on the preparative scale. First, total gliadins were extracted from defatted gluten by ethanol/water (70:30). Total gliadins recovered at this stage contained α/β, γ–, and ω-gliadins and small amounts of glutenins. Different chromatographic steps were then performed to obtain the γ_{46}-gliadins and "slow" ω-gliadin subfractions. (See the details of the purification procedure in Supporting Information.)

Purified "slow" ω- and γ_{46}-gliadins were characterized by acid and SDS-PAGE, reversed-phase HPLC (RP-HPLC), and mass spectrometry. Each purified gliadin exhibited only one band in electrophoresis and a single peak in RP-HPLC with expected migration and retention times (data not shown). The molar masses measured were 35 185 and 42 734 g/mol for γ_{46}-gliadins and "slow" ω-gliadins, respectively. The main characteristics of both prolamins are presented in Table 1.

In the present paper, γ_{46}-gliadins and "slow" ω-gliadins will be denoted γ-gliadins and ω-gliadins, respectively.

Surface Pressure-Area Isotherms. A Langmuir trough (Nima Technology, Coventry) equipped with a mobile barrier was used to prepare protein films. It was filled with a subphase consisting of a pH 7.2 50 mM phosphate buffer previously filtered through a glass microfibre filter (GF/F, Whatman). The water used was purified from a Milli-Q system (Millipore, Molsheim, France) with a nominal resistivity of 18.2 MΩ cm. Freeze-dried proteins were dissolved in a 52:48 (v/v) water/ethanol mixture at a concentration of C) 1 mg/mL and filtered through a 0.45 μm porosity filter (Millipore). The protein solutions were then spread at the air-water interface using a Hamilton microsyringe according to the Langmuir method. After an equilibrium time of about 10 min, the protein films were compressed at a speed of 10 cm^2/min, which correspond to 83 $Å^2$/ (molecule.min) for γ-gliadin and 50$Å^2$/(molecule.min) for ω-gliadin. The surface pressure (π) was monitored by a Wilhelmy surface balance using a filter paper plate (Whatman).

Brewster Angle Microscopy. The surfaces of the films were observed during compression using the BAM2 plus Brewster angle microscope (NFT, Göttingen, Germany) equipped with a frequency doubled Nd:YAG laser with a wavelength of 532 nm and a charge-coupled device camera with a 10X magnification lens. The exposure time (ET), depending on the image luminosity, was adjusted from 20 to 0.5 ms to avoid saturation of the camera. The spatial lateral resolution of the Brewster angle microscope was 2 μm, and the image size was 400 X 650 μm^2. The BAM images were coded in grey levels. To determine the thickness of the layer at the surface, the calibration procedure of the BAM software was used to determine the linear function between the reflectance and the grey level. This function was established by comparison between the experimental curve of the grey level as a function of the angle of incidence and the Fresnel curve (curve of the reflectance as a function of the angle of incidence) that can be fitted by a parabola around the Brewster angle minimum. From the reflectance value, the BAM thickness model allowed us to estimate the thickness of the layer at the surface with our knowledge of the experimental Brewster angle and the optical index of the film. This model is based on the proportionality relation between the reflectance and the square of the interfacial film thickness when the optical index of the film is assumed to be constant.[26] The approximate equation[27] for a thin, single-layered film is

$$R = \frac{I_R}{I_0} = (\pi \frac{d}{\lambda})^2 \frac{(n_1^2 - n_2^2 - 1 + \frac{n_2^2}{n_1^2})^2}{1 + n_2^2} \quad (1)$$

with I_0 and I_R being the incident and the reflected intensities, n_1 and n_2 being the refractive indices of the film (1) and the subphase (2), λ being the wavelength of the incident light, and d being the thickness of the film.

In this study, to obtain an approximation of the protein film thickness, the optical index of the gliadin films was assumed to be constant and equal to 1.47. This value was estimated for gliadin aqueous solutions that contain about 85% proteins.[28]

FTIR Spectroscopy. Absorbance spectra of solid gliadins in the bulk were obtained on a Nicolet Magma 550 spectrometer equipped with an MCT detector cooled at 77 K and germanium ATR crystal.

PM-IRRAS spectra were recorded on a Nicolet 870 Fourier transform infrared (FTIR) spectrometer by the co-addition of 600 scans at a resolution of 8 cm^{-1}. The details of the optical setup, the experimental procedure, and the two-channel processing of the detected intensity have been already described.[29] PM-IRRAS is a technique sensitive to the orientation of the transition moment at the water surface and hence the molecular groups themselves. In short, the surface selection rule indicates positive bands for transition moments lying in the surface plane whereas negative bands are attributed to transition moments perpendicular to the surface. For an intermediate orientation of the transition dipole moment, the two contributions are competing, and the absorption band vanishes when the transition dipole moment is tilted 39° from the surface normal of the water subphase. The PM-IRRAS device allows us to obtain the differential reflectivity spectrum

$$\Delta R/R = [(Rp-Rs)/(Rp+Rs)].J_2 \qquad (2)$$

with R_p being the p-polarized reflectance, R_s being the s-polarized reflectance, and J_2 being the Bessel function.

To remove the contribution of the subphase absorption and the dependence on the Bessel function, the film spectra are divided by that of the subphase. The water vapor contribution to the film spectra is removed by subtraction of the water vapor spectrum. The intensity of the absorbance bands is proportional to the surface concentration (N/A) and the orientation of the transition moment $f(\alpha)$.

$$I \propto N/A * f(\alpha) \qquad (3)$$

To obtain spectra independent of the surface concentration due to area reduction, spectra are multiplied by the surface area available for the film.

Simulation of PM-IRRAS Spectra. Simulated spectra have been obtained using a general software program developed for modeling the reflectivity of absorbing layered systems[30] and extended to anisotropic systems following the matrix method of Berreman.[31] The optical constants of water used for the simulations were obtained from Bertie and Lan,[32] and those of the secondary structure, from Buffeteau et al.[33] Simulation PM-IRRAS spectra of gliadins at the air-water interface was calculated by the combination of calculated secondary structure spectra of the α-helix, β-sheet, β-turn, and random coil. The original β-turn and random coil spectra are presented in Figure 1a. The α-helix and β-sheet have different PM-IRRAS spectra[34] according to their specific orientations relative to the interface. In the case of an α-helix, presented in Cornut et al.,[35] the amide I signal is dominated by the transition moment oriented parallel to the chain axis[36] (Az) absorbing at 1655 cm^{-1}. A strong positive amide I band and a weak positive amide II band, when the helix axis was parallel to the interface, ($\theta = 90°$) were noticed, and a negative amide I band with a strong positive amide II band appeared when the helix axis was perpendicular to the interface ($\theta = 0°$). β-Sheet structures present two amide I transition moments: the amide I′ at 1685 cm^{-1} oriented along the peptide chain and the amide I at 1625 cm^{-1}, corresponding to interchain hydrogen bonds, oriented perpendicular to the former. In the bulk state, the relative intensity ratio is $I_{AI}/I_{AI'} \sim 10$. The different orientations of â-sheet structures in relation to the interface are described by two angles: θ, the angle between the main peptide chain direction and the interface plane, and Ψ, the angle between the hydrogen bond direction and the interface plane. Three extreme orientations of the β-sheet can be distinguished:

(1) flat on the interface plane ($\theta = 0°$, $\Psi = 0°$), leading to a weak positive amide I′ band (1685 cm^{-1}) and a strong positive amide I band (1625 cm^{-1});

(2) perpendicular to the interface with peptide chains parallel to the interface ($\theta = 0°$, $\Psi = 90°$), leading to a positive amide I′ band and a strong negative amide I band;

(3) perpendicular to the interface with peptide chains perpendicular to the interface ($\theta = 90°$, $\Psi = 0°$), leading to a negative amide I′ band and a strong positive amide I band. Spectra of some principal orientations of β-sheet structures are illustrated in Figure 1b-d.

Results and Discussion

Compression Isotherms, Brewster Microscopy Observations, and Film Thicknesses. Under the conditions used, γ- and ω-gliadins instantaneously adsorb at the air-water interface after spreading. These homogeneous, stable films are depicted in Figure 2a,b and have uniform thickness without detectable defects at the resolution of the Brewster angle microscope. During compression, the protein films remain optically uniform and appear brighter and brighter. These changes in reflectance can be attributed to the optical index but mainly to film thickness changes. The film mobility indicates gel-like films, with the mobility being reduced with increasing compression. At a high level of compression, linear stripes can be observed in Brewster angle microscopy as illustrated in Figure 2c,d. The stripes are of micrometric width, and their thicknesses have nanometric variations. They may be attributed to the buckling of the monolayer.[37,38] Considering a constant optical index of 1.47 for the interfacial gliadins films, film thickness evolutions versus molecular areas were plotted in Figure 3. For both gliadins, the films thicknesses, roughly determined by our method, evolve from 1.5 to 9 nm. This thicknesses range is consistent with monolayer films given the molecular sizes of gliadins.[39] Thickness values are approximations; however, it can be observed that the thickness evolution can be described by the following equation

$$d = C.A^b \qquad (4)$$

where d is the film thickness, A is the molecular area, C is aconstant, and b is the exponent of the power law. On one hand, γ-gliadin thickness evolution is well fitted with the exponent $b = -1$, meaning that the interfacial volume can be considered to be constant during compression (Figure 3a). From this result, it can be concluded that there is no hydration change in the interfacial layer and no loss of proteins in the subphase during compression, considering a constant refractive index. The measured molecular volume is about 60nm^3/molecule;this value is low compared to the value previously obtained by small-angle X-ray scattering[39] on γ-gliadin in the bulk solubilized in a good solvent (.200 nm^3/molecule).

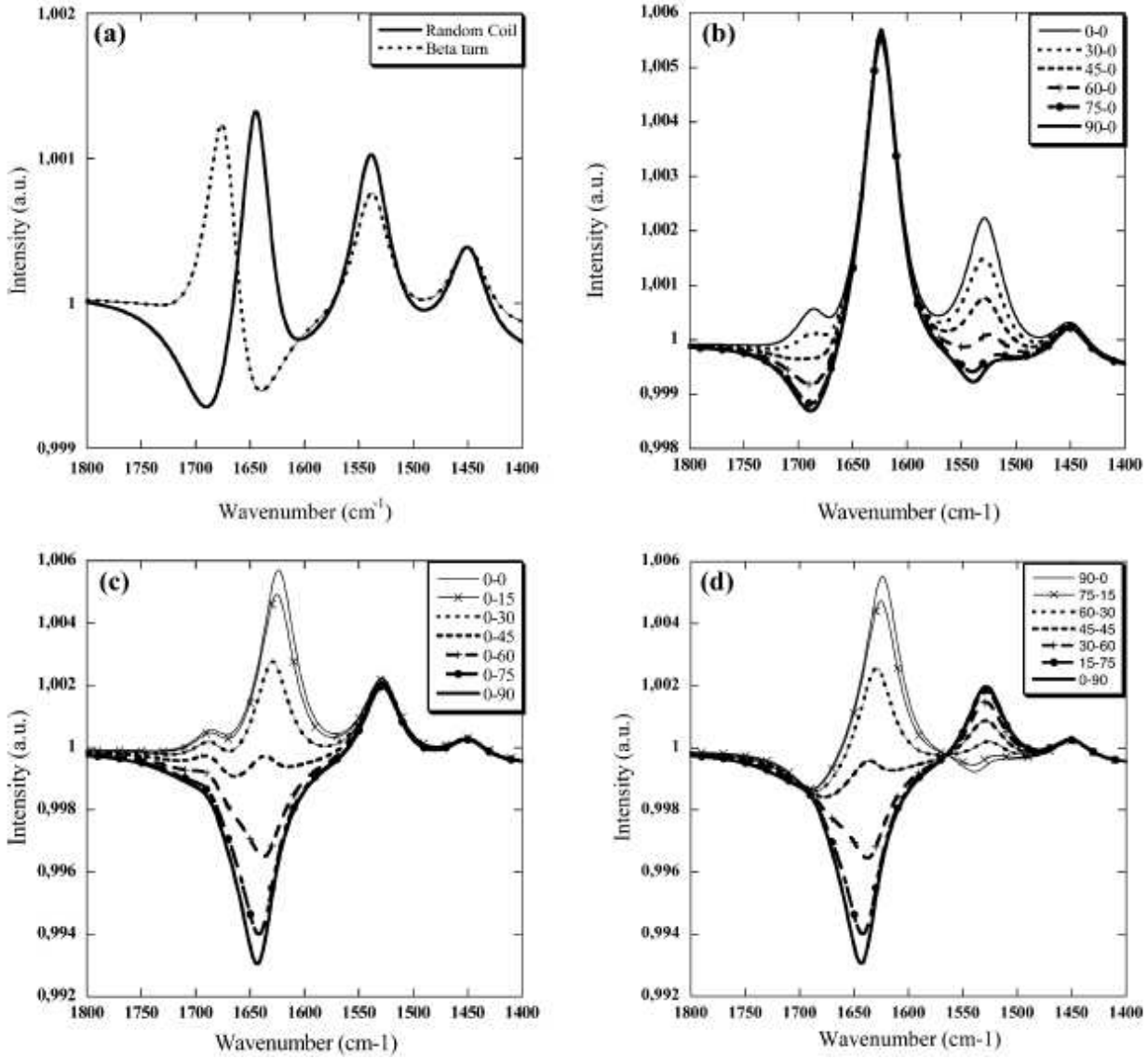

Figure 1. (a) Calculated PM-IRRAS spectra of isotropic β-turns and random coils. Calculated PM-IRRAS spectra of β-sheets with different orientations relative to the interface. (b) $0<\theta<90°$, $\psi = 0°$; (c) $\theta = 0°$, $0° < \psi < 90°$; (d) $0° < \theta < 90°$, $0° < \psi < 90°$.

This difference can be attributed to various conformations adopted by γ-gliadin under different solvent conditions. It has previously been observed that γ-gliadin was more extended in good solvents.[40] Moreover, the γ-gliadin volume measured at the air-water interface is consistent with the volume calculated for folded soluble proteins with the same range of molecular weight.[41]

However, the experimental data for ω-gliadin thickness evolution can be well fitted with exponent b = -0.6 (Figure 3.b). This exponent value means that the interfacial film volume evolves with the area as follows:

$$V=d.A= C.\ A^{0,4} \quad (5)$$

Therefore, the film volume decreases as the area decreases assuming a constant film refractive index. This evolution can be attributed to a loss of ω-gliadins into the subphase or to a densification of the interfacial layer. The compression isotherms of γ- and ω-gliadins at the air-water interface are also presented in Figure 3. They exhibit slope changes that define three regimes for γ-gliadin and two regimes for ω-gliadin. At high molecular areas, the slopes are weak, then in the second regime, the slopes increase when reducing the molecular area. This behaviour looks like the 2D phase transition of simple molecules, from an expanded liquid phase to a condensed liquid phase. In the third step of the γ-gliadin isotherm, the slope of the interfacial pressure is lower than in the second step. According to thickness measurements, the hypothesis of stacking of γ-gliadin structures should be retained and not result in a loss of γ-gliadin into the subphase.

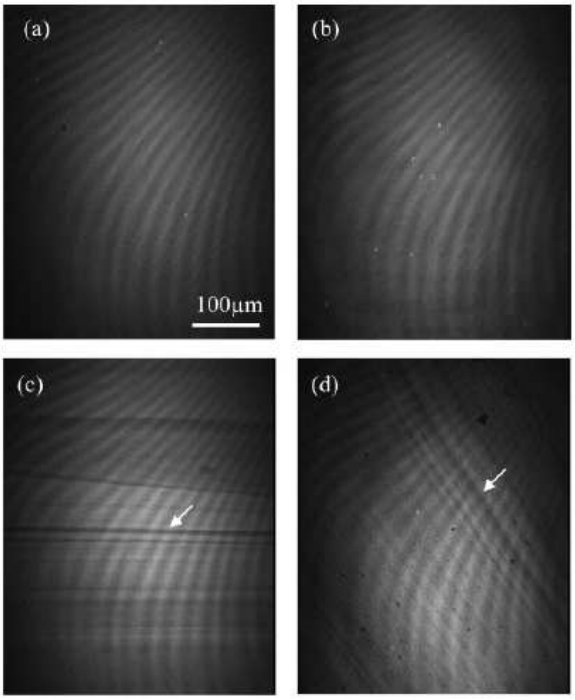

Figure 2. Brewster angle microscopy images of gliadins at the air-water interface. (a) γ-gliadins, π= 6 mN/m, ET = 1/50 s, GL = 100; (b) ω-gliadins, π= 6.7 mN/m, ET = 1/50 s, GL = 106; (c) γ-gliadins, π= 29 mN/m, ET = 1/1000 s, GL = 120; (d) ω-gliadins,π= 15 mN/m, ET=1/2000 s,GL=130. (π, interfacial pressure; GL, gray level; ET, exposure time).

In addition, preliminary experiments (data not shown), in which the interfacial pressure was measured as a function of the quantity of proteins injected into the subphase, indicated that the interfacial pressure stabilizes at π=21 mN/m for γ-gliadins and π=10 mN/m for ω-gliadins. These pressures are obtained at the beginning of the last steps of the compression isotherms, suggesting that the last steps are unstable. This instability is confirmed in these compression ranges by the decrease in interfacial pressure when barrier movement is stopped. Moreover, during experiments this instability was correlated with the apparition of the linear stripes in microscopy as observed in Figure 2c,d.

Structures of Solid Gliadins by FTIR (ATR). Gliadin infrared spectra have been presented many times but often exclusively in the amide I and amide II regions.[13-15] Figure 4 displays solid γ- and ω–gliadin infrared spectra in the 1300-1800 cm^{-1} range, where amide bands at 1550 and 1650 cm^{-1} and an intense band at 1450 cm^{-1} are reported. Some authors assigned the band at 1450 cm^{-1} to CH stretching of the pyroindoline ring; however, considering the high rate of proline in gliadins, this band could rather be assigned to CN vibrations in proline residues. Indeed, only a few authors[42-44] corrected the attribution of this intense band also observed in the polyproline spectra. Moreover, the integrated area of this peak normalized by the amide I band integrated area appears proportional to the proline content of each gliadin fraction (17.5% of proline in γ-gliadin[45] and 29% in ω-gliadin).[46] The high proline content also explains the variable area of the amide II band because this residue does not display the amide II mode. As previously observed, γ-gliadin amides bands are dominated by α-helix bands at 1651 and 1540 cm^{-1}, whereas ω-gliadin amide bands are shifted toward lower wavelengths by β-structures. A significant contribution at 1651 cm^{-1} can be observed in ω–gliadin spectra. This contribution was interpreted differently by the authors.

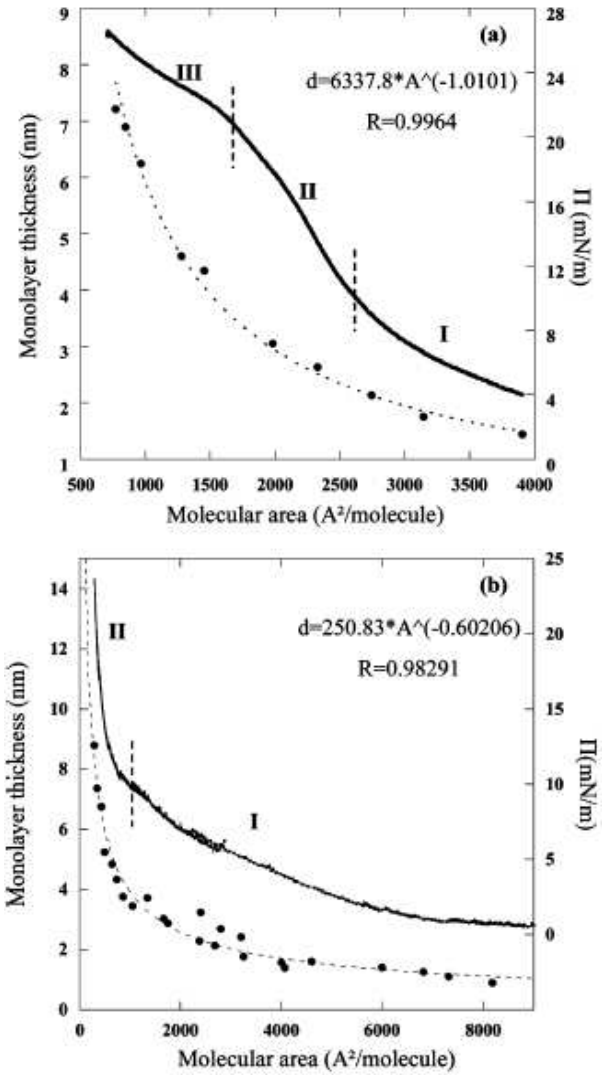

Figure 3. Compression isotherms (full line) and interfacial film thicknesses versus molecular area: experimental (dots) and theoretical (dashed line) using eq 4 (see text). (a) γ-Gliadins and (b) ω-gliadins.

Pezolet et al.[14] attributed it, classically, to α-helices whereas other authors refuted this hypothesis because no α-helices were detected by CD spectra[47] and the very high content of proline in ω-gliadins would not favour α–helix structures formation. Therefore, Wellner et al.[15] attributed this contribution to the high content of glutamine residues in ω–gliadin. However, the α-helix conformation can be taken into account because glutamine residues have a good propensity to form helices,[48] and it has been suggested that proline is perhaps better described as a α-helix initiator rather than a helix breaker.[49] Therefore, small α-helices could be hypothetically formed between proline residues. Large loops connecting β-structures[50,51] can also be proposed. This last

hypothesis is reinforced by a molecular dynamics study on an octapeptide repeat of the ω-gliadin repetitive domain that displays an original interpenetrating folding pattern containing β-sheets and turns.[52]

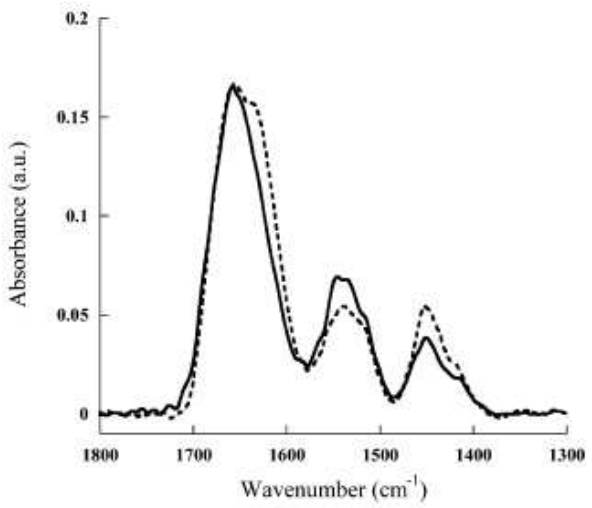

Figure 4. IR absorption spectra of solid ω-gliadin (dashed line) and γ-gliadin (full line).

Structures of Gliadins by PM-IRRAS at the Air/Water Interface. PM-IRRAS spectra of gliadins at the air-water interface exhibit amides absorption bands, CN vibration band of prolines, and few low-intensity bands in the 1000-1300 cm^{-1} region. In this last region, there are two positive bands at 1244 (very weak) and 1067 cm^{-1} and a negative band at 1090 cm^{-1} (Figure 5). These bands are attributed to phosphate salts from the subphase: 1244 and 1067 cm^{-1} bands are assigned to PO_2^- asymmetrical and symmetrical vibrations, respectively, and the 1090 cm^{-1} band is assigned to the asymmetrical PO_3^{2-} vibration. Because gliadin spectra are divided by those of the subphase, these bands indicate an increase in the PO_2^-/PO_3^{2-} ratio at the interface and thus an acidification of the interfacial pH with the addition of gliadins.

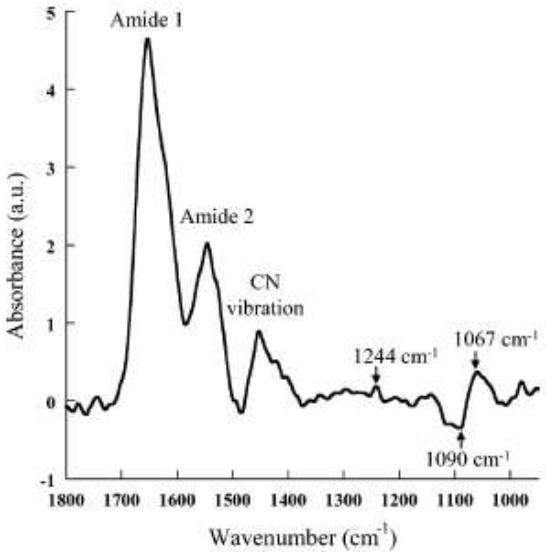

Figure 5. Typical PM-IRRAS spectrum of gliadins at the air-water interface.

γ-gliadin structure. Figure 6 presents isotherm curves and PM-IRRAS spectra of pure γ-gliadin films at the air-water interface obtained along the compression of the film. Results were obtained in two different experiments with different quantities of γ-gliadin injected at the air-water interface to cover a large range of molecular areas. In the first experiment, in the high-molecular-area regime (spectra 1 and 2 in Figure 6), the amide I band is split into two main bands, one at 1653 cm^{-1} attributed to α-helices and another at 1669 cm^{-1} attributed to β-turns. Contributions at 1685 and 1619 cm^{-1} due to antiparallel β-sheets and at 1635 cm^{-1} due to parallel β-sheet structures are also observed. The high proportion of β-turns can be attributed to a low folded state of the protein.[53] With increasing compression (spectra 2-4), the α-helix contribution at 1653 cm^{-1} becomes more important. γ-gliadin molecules that initially have low structure at the air-water interface may be refolded under compression. This behavior was previously observed with other proteins at the air-water interface.[54] The second and third steps of the isotherm (spectra 4-9) were acquired in a second experiment in which the initial quantity of gliadins injected at the air-water interface was more important. The last spectra of the first experiment (spectrum 3) and the first spectra of the second experiment (spectrum 4) are reasonably correlated, but a frequency shift of the α-helix contribution is observed (from 1653 to 1658 cm^{-1}). According to Nevskaya and Chirgadze,[55] the frequency of α-helices steadily rises when the number of amino acid residues involved in α-helical structures decreases. α-helices should thus be longer at the end of the first regime than at the beginning of the second one. This behavior can be explained by the fact that in the first experiment gliadins can progressively fold along compression whereas in the second experiment protein foldingmaybe hindered by the high concentration directly injected at the interface. During the second and the third steps of the isotherm, no major modifications of γ-gliadin spectra at the interface are noticed. However, a progressive shift of the amide I maximum (from 1658 to 1655 cm^{-1}) with compression can be observed and attributed to low α-helix lengthening. Moreover, between 2500 and 1500 $Å^2$/molecule (spectra 4-6), the appearance and the increase in the bands at 1645 and 1628 cm^{-1} assigned to random coils and β-sheets, respectively, are also noticed. Parallel β-sheet formation must be the result of intermolecular interactions whereas helix lengthening is attributed to γ-gliadin structuring in response to the lack of space at the interface. It was previously observed[14] that functional gluten proteins in the doughy state contain more intra- and intermolecular β-sheets and fewer β-turns and α-helices than in an acetic acid solution where gliadin are partially unfolded. At the lower molecular areas, between 1500 and 400$Å^2$/molecule, the compression isotherm is modified by the stop of the mobile barrier. During spectra acquisition time, there is a decrease in interfacial pressure that may be due to the film relaxation. In the last step of the isotherm (spectra 7-9), secondary structures remain unchanged. Besides, the normalized CN vibration bands have nearly constant areas.

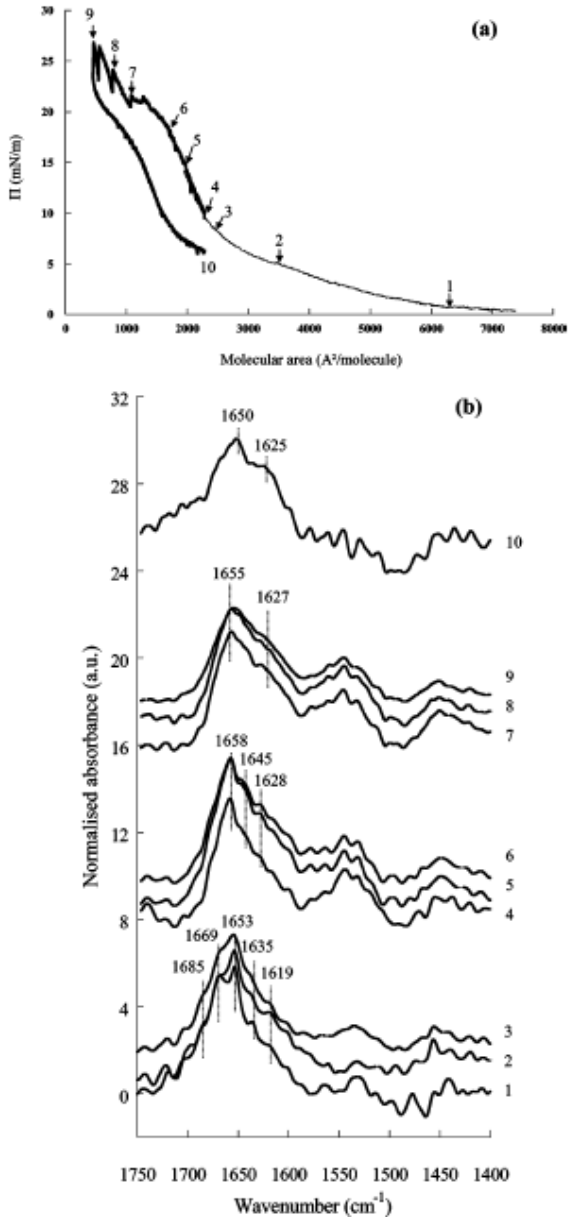

Figure 6. PM-IRRAS spectra of γ-gliadins at the air-water interface. (a) Compression isotherms at the air-water interface (performed in two different experiments) and localization of PMIRRAS acquisitions. (b) PM-IRRAS spectra pooled according to the isotherm regimes.

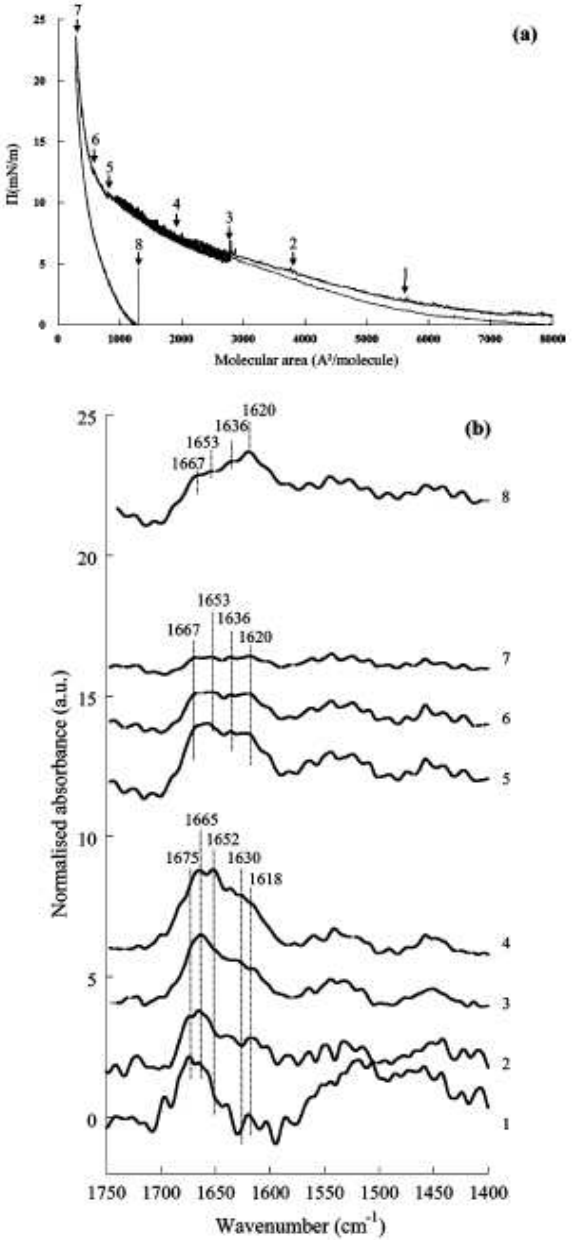

Figure 7. PM-IRRAS spectra of ω-gliadins at the air-water interface. (a) Compression isotherms at the air-water interface (performed in three different experiments) and localization of PMIRRAS acquisitions. (b) PM-IRRAS spectra pooled according to the isotherm regimes.

This means that the interfacial gliadin concentration, normalized by the molecular area, is constant, as the area of the CN vibration band should be proportional to the gliadin concentration at the interface, contrary to amide bands that can be modified by specific orientations of secondary structures. It confirms that γ-gliadins are fully maintained at the interface, even at very high compression levels. Decompression was carried out in the second experiment. Hysteresis can be observed on the pressure isotherm, and it can be attributed to the slow relaxation of the interfacial film. Spectrum 10 shows that after decompression the interfacial film does not recover its initial structure. The amide I band is characterized by important contributions at 1665, 1650, and 1625 cm^{-1}, attributed to β-turns, long α-helices, and β-sheets, respectively. There is a very low contribution of random coils (1640 cm^{-1}). Only secondary structures stabilized by hydrogen bonds are maintained after decompression. In addition, information concerning the orientation of secondary structures can be obtained using the amide I/amide II band intensity ratio (I_{AI}/I_{AII}). The PM-IRRAS spectra of γ-gliadins in the high-molecular-area regime (spectra 1 and 2) display a low-intensity amide II band whereas amide I is intense. This uncommon intensity ratio cannot be explained by the β-turns contribution because these small secondary structures cannot massively orientate relative to the interface.

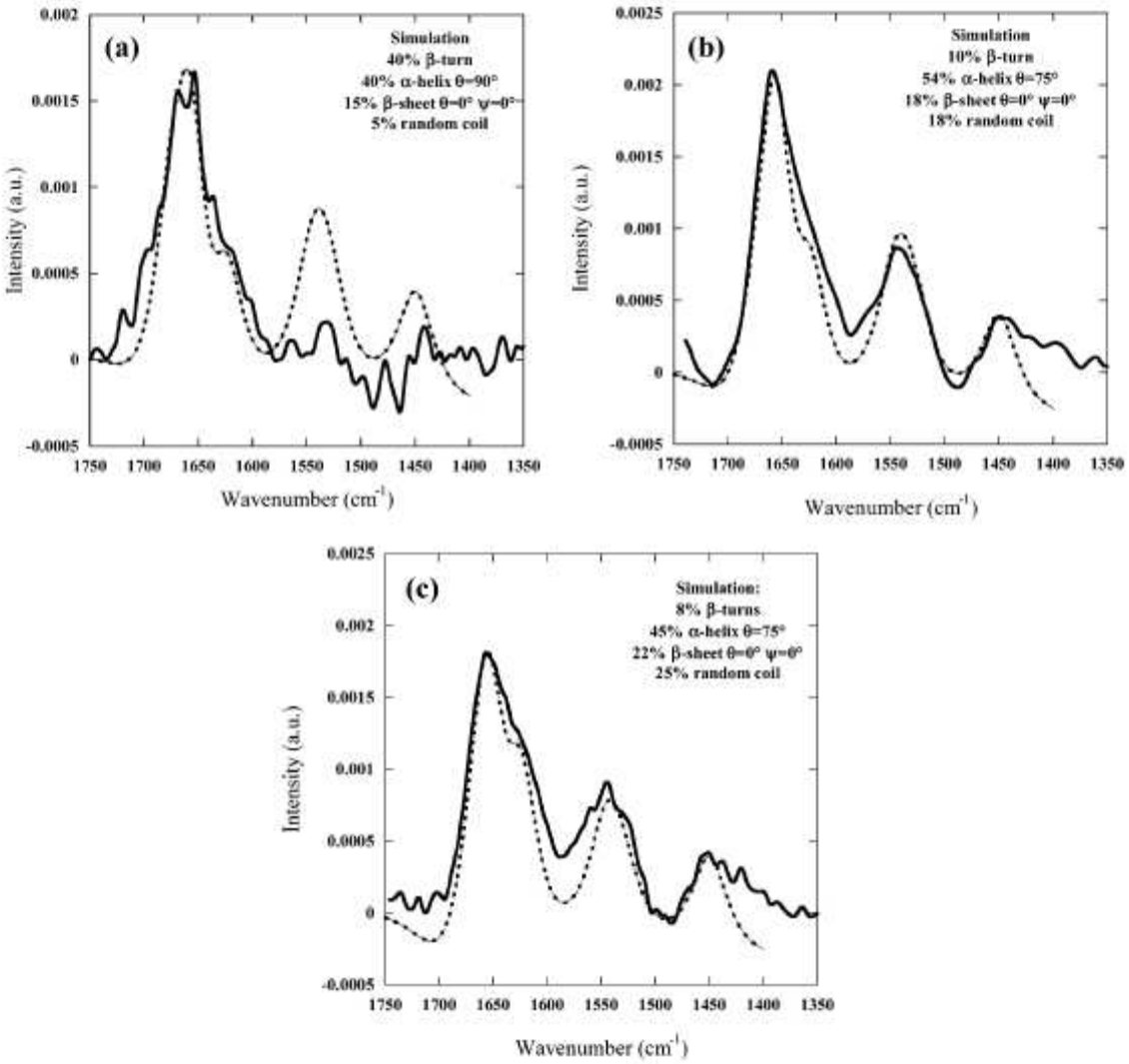

Figure 8. Calculated (dashed lines) and measured (full lines) PM-IRRAS spectra of γ-gliadin at the air-water interface at low and high compression levels.(a) At 6000 Å^2/molecule, the calculated spectrum is a combination of 40% α-helices oriented parallel to the interface, 15% β-sheets oriented flatly with respect to the interface, 5% random coils, and 40% β-turns. (b) At 2300 Å^2/molecule, the calculated spectrum is a combination of α-helices oriented at $\tilde{o}$) 75°, 18% β-sheets oriented flatly with respect to the interface, 18% random coils, and 10% β-turns. (c) At 600 Å^2/molecule, the calculated spectrum is a combination of 45% α-helices oriented at $\tilde{o}$) 75°, 22% β-sheets oriented flatly with respect to the interface, 25% random coils, and 8% β-turns.

This ratio must be essentially due to the α-helix orientation. Taking into account the PM-IRRAS spectra simulations of α-helices,[35] the very low intensity of the amide II band indicates the flat orientation of the α-helix in relation to the interface. In very high molecular areas, structures are thus flat on the interface. In the first regime of the isotherm, the amide I/amide II ratio decreases from 7 to 4.7. This result can be attributed to the weak reorientation of α-helices, from 90 to 75° in relation to the normal of the interface. Finally, in the second and the third regimes, no orientation changes can be deduced.

ω-gliadin Structure. Figure 7 presents the PM-IRRAS spectra of pure ω-gliadin films at the air-water interface along compression. This plot is the result of three different experiments represented by the different grey levels of the pressure isotherms (Figure 7a). For low molecular areas (spectra 1 and 2), amide bands are noisy and disturbed by a negative band between 1550 and 1650 cm^{-1}. It is attributed to the very low protein concentration and the perturbation of the interfacial water by the hydrated proteins, combined with an optical effect.[29,56,57] Briefly, the optical effect is credited to the water absorption band, centred at approximately 1640 cm^{-1}, corresponding to the position where the PM-IRRAS spectrum abruptly changes, showing a positive band immediately followed by a negative band. This behaviour is due to an abrupt variation in the refractive index of the aqueous subphase in this range of frequencies. The amide I signal on spectra 2 and 3 has contributions around 1665 and 1620 cm^{-1} that can be assigned to β-turns in water.[58] The contribution at 1630 cm^{-1} is attributed to β-sheets. The increase in the contribution at 1652 cm^{-1}, represented on spectra 4, can be attributed to glutamine and α-helices or large loops, as discussed before.

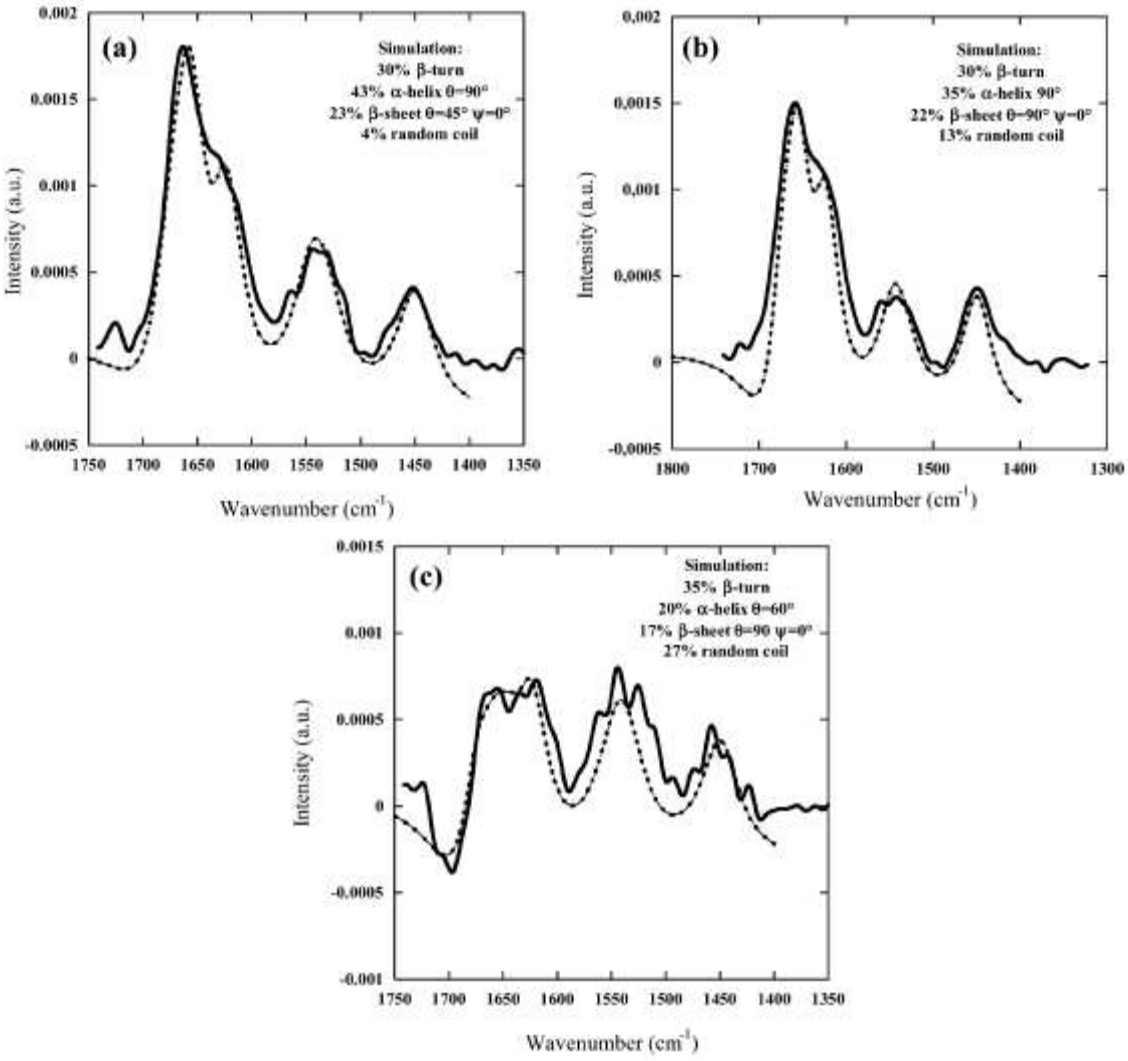

Figure 9. Calculated (dashed line) and measured (full line) PM-IRRAS spectra of ω–gliadins at the air-water interface at different compression levels. (a) At 6000 Å^2/molecule, the calculated spectrum is a combination of 43% α-helices oriented parallel to the interface, 23% β-sheets oriented at θ= 45°, 4% random coils, and 30% β-turns. (b) At 3000 Å^2/molecule, the calculated spectrum is a combination of 35% α-helices oriented parallel to the interface, 22% β-sheets oriented at θ=90°, 13% random coils, and 30% β-turns. (c) At 600Å^2/molecule. the calculated spectrum is a combination of 20% α-helices oriented at θ= 60° relative to the normal of the interface, 17% β-sheets oriented at θ= 90°, 27% random coils. and 35% β-turns.

The evolution of ω-gliadin spectra along compression (spectra 1-4) demonstrates that ω-gliadins contain more long structures at the end of the first domain, either β-sheets and α-helices, or large loops made of β-sheets. During the first domain of the isotherm, ω-gliadins, like γ-gliadins, are initially low folded at the air-water interface (numerous β-turns) and then fold with compression. In the second step of the isotherm (spectra 5-7), amide I peak is more and more dominated by contributions at low frequencies (1620-1630 cm^{-1} region), assigned to β-sheets. With a small molecular area available, proteins should be forced to interact mutually through β-sheet interactions. Concurrently, amide bands and CN vibrational band intensities significantly decrease. This result confirms that ω-gliadin molecules are forced out of the monolayer, as previously deduced from the film thickness evolution along compression. Decompression was carried out for the third experiment, and a zero surface pressure was obtained, meaning that ω-gliadin molecules have been lost in the subphase. The PM-IRRAS spectrum acquired after decompression and 1 h of equilibration time (spectrum 8) shows a protein signal. Even if it is noisy, the amide I band shape is very different from the spectrum acquired before compression. ω-Gliadin does not recover its initial structure, with the amide I signal being dominated by antiparallel β-sheets (1620 cm^{-1}) and parallel β-sheets (1636 cm^{-1}) (spectrum 8). Less important contributions of helices (1653 cm^{-1}) and β-turns (1667 cm^{-1}) are also observed. The majority of ω-gliadin organized structures are maintained after decompression, as with γ-gliadins.

Simulation of PM-IRRAS Spectra. To confirm the interpretation of PM-IRRASresults, spectra were fitted with a combination of α-helix, β-sheet, β-turn, and random coil calculated spectra. These simulations were performed to give some trends of the general behaviour of secondary structures

along compression. Simulations of γ-gliadin PM-IRRAS spectra obtained at 6000, 2300, and 600Å2/molecule fit the experimental spectra reasonably well (Figure 8). However, a discrepancy between simulated and experimental spectra is noticed between the simulated and the experimental amide II bands in Figure 8a, which corresponds to the γ-gliadin monolayer at 6000 $Å^2$/molecule. Experimentally, this band may be hidden by the negative band of the perturbed interfacial water that is relatively important at low protein surface concentration. On the basis of the simulations, it can be postulated that at high molecular area most of the α-helices and β-sheets of γ-gliadin are oriented flat on the water surface (Figure 8a). Upon further compression, the simulated spectra suggest that most β-turns are transformed into random coils and α-helices, with the helices having rotated to an angle of 75° relative to the normal of the interface (Figure 8b). At lower molecular area (Figure 8c), the simulated data allow us to speculate that the proportion of random coils and β-sheets slightly increases at the expense of the α-helices, although the observed changes are rather small. Simulations thus suggest weak orientation changes of α-helices in the first domain of compression and small changes in the proportion of the different secondary structure components in both first domains. Generally, there is a decrease in the wavelength of the amide I contributions from 1670 to 1625 cm^{-1}, which suggests an increase in β-sheets at the expense of β-turns. Simulated ω-gliadin spectra fit the experimental data reasonably well. On the basis of these simulations, it can be postulated that at high molecular area ω-gliadin secondary structure is dominated by β-turns and α-helices with flat orientation relative to the interface (Figure 9a). β-Sheets are well fitted with an orientation of $\theta = 45°$, $\psi = 0°$ that corresponds to the hydrogen bond direction parallel to the interface and the main peptide chain direction oriented at an angle of $\theta = 45°$ relative to the interface. Upon compression, the simulated spectra suggest that the content of each secondary structure does not evolve but the orientation of β-sheets changes (Figure 9b). The orientation $\theta = 90°$, $\psi = 0°$ means vertical orientation of the main peptide chain direction. At very low molecular area, the specific PMIRRAS spectra of ω-gliadin is well fitted with a combination of β-turns and β-sheets perpendicular to the interface with the hydrogen bond direction parallel to the interface, α-helices oriented at an angle of $\theta = 60°$ relative to the normal of the interface, and random coils (Figure 9c). Therefore, simulations suggest that during the first regime there is a rotation of β-structures, which leads to a more compact arrangement, and during the second regime there is a standing up of helices and a decrease in their content to the profit of random coils.

Conclusions

γ- and ω-gliadins form homogeneous monolayers at the airwater interface. At high molecular areas, these proteins are low folded and secondary structures are oriented flat relative to the interfacial plane. In the first steps of compression, the γ-gliadins film stability seems to be maintained by small changes in secondary structures and orientations. The β-turn content decreases at the expense of β-sheets, leading to the hypothesis that the compression induces the formation of intermolecular β-sheets, which would enable us to bring molecules into close contact for assembly. Upon further compression, a model of γ-gliadin stacking in the direction perpendicular to the interface is proposed. This result is in agreement with the polymer scaling concept analysis done on gliadin isotherms by Hargreaves et al.[59] However, ω-gliadins are less stable at the air-water interface. Upon compression, secondary structures rotate to minimize the interfacial area, and then ω-gliadin molecules are forced out of the monolayer. Contrary to γ-gliadins, ω-gliadins are not able to accumulate at the air-water interface. These different behaviours can be explained by the different polarities of both amino acid chains. According to the primary structure of γ-gliadins, the C-terminal, nonrepetitive domain would be responsible for the high surface activity of these proteins, whereas the ω-gliadin behavior seems to indicate that the repetitive domain has the ability to organize itself by the rotation of secondary structures. These interfacial properties under compression may thus be relevant for a biological purpose such as the natural accumulation of these proteins in protein bodies. Future work will be devoted to the study of these gliadins at the water-membrane (made with lipids) interface to closely mimic the biological context of the accumulation of these proteins.

Acknowledgment. We acknowledge financial support from INRA and CNRS within the framework of the Groupement De Recherches “Assemblages de Macromolécules Végétales”, and we are grateful to Jean-Pierre Compoint and Dominique Melcion for the purification of the gliadins.

Bibliography

(1) Sliwinski, E. L.; Kolster, P.; Prins, A.; van Vliet, T. *J. Cereal Sci.* **2004**, *39*, 247-264.
(2) Pallos, F.; Robertson, G.; Pavlath, A.; Orts, W. *J. Agric. Food Chem.* **2006**, *54*, 349-352.
(3) Ezpeleta, I.; Irache, J. M.; Stainmesse, S.; Chabenat, C.; Gue´guen, J.; Popineau, Y.; Orecchioni, A. M. *Int. J. Pharm.* **1996**, *131*, 191-200.
(4) Galili, G. *Plant Physiol.* **2004**, *136*, 3411-3413.
(5) Vitale, A.; Ceriotti, A. *Plant Physiol.* **2004**, *136*, 3420-3426.
(6) Shewry, P. R.; Halford, N. G. *J. Exp. Bot.* **2002**, *53*, 947-958.
(7) Tatham, A. S.; Shewry, P. R. *J. Cereal Sci.* **1995**, *22*, 1-16.
(8) Bietz, J. A.; Burnouf, *T. Theor. Appl. Genet.* **1985**, *70*, 599-608.
(9) Blanch, E.; Kasarda, D.; Hecht, L.; Nielsen, K.; Barron, L. *Biochemistry* **2003**, *42*, 5665-5673.
(10) Georget, D. M. R.; Belton, P. S. *Biomacromolecules* **2006**, *7*, 469-475.
(11) Wellner, N.; Mills, E. N. C.; Brownsey, G.; Wilson, R. H.; Brown, N; Freeman, J.; Halford, N. G.; Shewry, P. R.; Belton, P. S. *Biomacromolecules* **2005**, *6*, 255-261.
(12) Mangavel, C.; Barbot, J.; Popineau, Y.; Guéguen, J. *J. Agric. Food Chem.* **2001**, *49*, 867-872.
(13) Blanch, E.; Kasarda, D.; Hecht, L.; Nielsen, K.; Barron, L. *Biochemistry* **2003**, *42*, 5665-5673.
(14) Pezolet, M.; Bonenfant, S.; Dousseau, F.; Popineau, Y. *FEBS Lett.* **1992**, *299*, 247-250.
(15) Wellner, N.; Belton, P. S.; Tatham, A. S. *Biochem. J.* **1996**, *319*, 741- 747.

(16) Tatham, A. S.; Masson, P.; Popineau, Y. *J. Cereal Sci.* **1990**, *11*, 1-13.
(17) Lullien-Pellerin, V.; Popineau, Y.; Meersman, F.; Morel, M.-H.; Heremans, K.; Lange, R.; Balny, C. *Eur J. Biochem.* **2001**, *268*, 5701-5712.
(18) Ornebro, J.; Nylander, T.; Eliasson, A.-C. *J. Cereal Sci.* **2000**, *31*, 195- 221.
(19) Ornebro, J.; Nylander, T.; Eliasson, A.-C.; Shewry, P. R.; Tatham, A. S.; Gilbert, S. M. *J. Cereal Sci.* **2003**, *38*, 147-156.
(20) Keller, R. C. A.; Orsel, R.; Hamer, R. J. *J. Cereal Sci.* **1996**, *25*, 175-183.
(21) Ornebro, J.; Nylander, T.; Eliasson, A.-C.; Shewry, P. R.; Tatham, A. S.; Gilbert, S. M. *J. Cereal Sci.* **2001**, *34*, 141-150.
(22) Ornebro, J.; Wahlgren, M.; Eliasson, A.-C.; Fido, R. J.; Tatham, A. S. *J. Cereal Sci.* **1999**, *30*, 105-114.
(23) Wannerberger, L.; Nylander, T.; Eliasson, A.-C.; Tatham, A. S.; Fido, R. J.; Miles, M. J.; McMaster, T. J. *J. Cereal Sci.* **1997**, *26*, 1-13.
(24) Triulzi, R. C.; Li, C.; Naistat, D.; Orbulescu, J.; Leblanc, R. M. *J. Phys. Chem. C* **2007**, *111*, 4661-4666.
(25) Lepère, M.; Chevallard, C.; Hernandez, J. F.; Mitraki, A.; Guenoun, P. *Langmuir* **2007**, *23*, 8150-8155.
(26) de Mul, M. N. G.; Mann, J. A. *Langmuir* **1998**, *14*, 2455-2466.
(27) Winsel, K.; Honing, D.; Lunkenheimer, K.; Geggel, K.; Witt, C. *Eur. Biophys. J.* **2003**, *32*, 544-552.
(28) Brailsford Robertson, T.; Greaves, J. E. *J. Biol. Chem.* **1911**, 181-184.
(29) Blaudez, D.; Turlet, J. M.; Dufourcq, J.; Bard, D.; Buffeteau, T.; Desbat, B. *J. Chem. Soc., Faraday Trans.* **1996**, *92*, 525-530.
(30) Buffeteau, T.; Desbat, B. *Appl. Spectrosc.* **1989**, *43*, 1027-1032.
(31) Berreman, D. W. *J. Opt. Soc. Am.* **1972**, *62*, 502-510.
(32) Bertie, J. E.; Lan Z. *Appl. Spectrosc.* **1996**, *50*, 1047-1057.
(33) Buffeteau, T.; le Calvez, E; Castano, S.; Desbat, B.; Blaudez, D.; Dufourcq, J. *J. Phys. Chem. B* **2000**, *104*, 4537-4544.
(34) Castano, S.; Desbat, B.; Laguerre, M.; Dufourcq, J. *Biochim. Biophys. Acta* **1998**, *1416*, 176-194.
(35) Cornut, I.; Desbat, B.; Turlet, J. M.; Dufourcq, J. *Biophys. J.* **1996**, *70*, 305-312.
(36) Miyazawa, T. *Infrared Spectra and Helical Conformations*; Marcel Dekker: New York, 1967.
(37) Bourdieu, L.; Daillant, J.; Chatenay, D.; Braslau, A.; Colson, D. *Phys. Re*V*. Lett.* **1994**, *72*, 1502.
(38) Fontaine, P.; Daillant, J.; Guenoun, P.; Alba, M.; Braslau, A.; Mays, J. W.; Petit, J. M.; Rieutord, F. *J. Phys. II France* **1997**, *7*, 401-407.
(39) Thomson, N. H.; Miles, M. J.; Popineau, Y.; Harries, J.; Shewry, P. R.; Tatham, A. S. *Biochim Biophys. Acta* **1999**, *1430*, 359-366.
(40) Orecchioni, A. M.; Duclairoir, C.; Renard, D.; Nakacke, E. *J. Nanosci. Nanotechnol.* **2006**, *6*, 3171-3178.
(41) Uversky, V. N. *Cell. Mol. Life Sci.* **2003**, *60*, 1852-1871.
(42) Rothschild, K. J.; He, Y.-W.; Gray, D.; Roepe, P. D.; Pelletier S. L.; Brown R. S.; Herzfeld *J. Proc. Natl. Acad. Sci. U.S.A.* **1989**, *86*, 9832-9835.
(43) Gerwert, K.; Hess, B.; Engelhard, M. *FEBS Lett.* **1989**, *261*, 449-454.
(44) Caswell, D. S.; Spiro, T. G. *J. Am. Chem. Soc.* **1987**, *109*, 2796-2800.
(45) Popineau, Y.; Pineau, F. *J. Cereal Sci* **1985**, *3*, 363-378.
(46) Popineau, Y.; Le Guerroué, J. L.; Pineau, F. *Lebensm. Wiss. Uni*V*. Technol.* **1986**, *19*, 266-271.
(47) Tatham, A. S.; Shewry, P. R. *J. Cereal Sci.* **1985**, *3*, 103-113.
(48) Park, S. H.; Shalongo, W.; Stellwagen, E. *Biochemistry* **1993**, *32*, 7048- 7053.
(49) Richardson, J. S.; Richardson, D. C. *Science* **1988**, *240*, 1648-1652.
(50) Malin, E. L.; Alaimo, M. H.; Brown, E. M.; Aramini, J. M.; Germann, M. W.; Harold, M. F.; McSweeney, P. L. H.; Fox, P. F. *J. Protein Chem.* **2001**, *20*, 391-404.
(51) Wilder, C. L.; Friedrich, A. D.; Potts, R. O.; Daumy, G. O.; Francoeur, M. L. *Biochemistry* **1992**, *31*, 27-31.
(52) Areas, E. P. G.; Cassiano, M. M. *Biophys. Chem.* **2001**, *90*, 135-146.
(53) Smith, T. F. *Nature* **1995**, *268*, 959-961.
(54) Lavoie, H.; Gallant, J.; Grandbois, M.; Blaudez, D.; Desbat, B.; Boucher, F.; Salesses, C. *Mater. Sci. Eng. C* **1999**, *10*, 147-154.
(55) Nevskaya, N. A.; Chirgadze, Y. N. *Biopolymers* **1976**, *15*, 637-648.
(56) Lavoie, H.; Blaudez, D.; Vaknin, D.; Desbat, B.; Ocko, B.; Salesses, C. *Biophys. J.* **2002**, *83*, 3558-3569.
(57) Granbois, M.; Desbat, B.; Salesse, C. *Biophys. Chem.* **2000**, *88*, 127- 135.
(58) Mantsch, H. H.; Perczel, A.; Hollosi, M.; Fasman, G. D. *Biopolymers* **1993**, *33*, 201-207.
(59) Hargreaves, J.; Douillard, R.; Popineau, Y. In *Food Macromolecules and Colloids*; Dickinson, E., Lorient, D., Eds.; Royal Society of Chemistry: Cambridge, U.K., 1995; pp 71-76.